

Intercomparison exercise between different radiative transfer models used for the interpretation of ground-based zenith-sky and multi-axis DOAS observations

F. Hendrick¹, M. Van Roozendael¹, A. Kylling^{2,*}, A. Petritoli³, A. Rozanov⁴, S. Sanghavi⁵, R. Schofield^{6,**}, C. von Friedeburg⁵, T. Wagner⁵, F. Wittrock⁴, D. Fonteyn¹, and M. De Mazière¹

¹Institut d'Aéronomie Spatiale de Belgique, Brussels, Belgium

²Norwegian Institute for Air Research, Kjeller, Norway

³Institute of Atmospheric Science and Climate, Bologna, Italy

⁴Institute of Environmental Physics, University of Bremen, Bremen, Germany

⁵Institute of Environmental Physics, University of Heidelberg, Heidelberg, Germany

⁶National Institute of Water and Atmospheric Research, Omakau, Central Otago, New Zealand

* now at: St. Olavs University Hospital, Trondheim, Norway

** now at: NOAA Aeronomy Laboratory, Boulder, Colorado, USA

Received: 30 June 2005 – Published in Atmos. Chem. Phys. Discuss.: 2 September 2005

Revised: 29 November 2005 – Accepted: 13 December 2005 – Published: 20 January 2006

Abstract. We present the results of an intercomparison exercise between six different radiative transfer (RT) models carried out in the framework of QUILT, an EU funded project based on the exploitation of the Network for the Detection of Stratospheric Change (NDSC). RT modelling is an important step in the interpretation of Differential Optical Absorption Spectroscopy (DOAS) observations. It allows the conversion of slant column densities (SCDs) into vertical column densities (VCDs) using calculated air mass factors (AMFs). The originality of our study resides in comparing SCD simulations in multi-axis (MAX) geometry (trace gases: NO₂ and HCHO) and in taking into account photochemical enhancement for calculating SCDs of rapidly photolysing species (BrO, NO₂, and OClO) in zenith-sky geometry. Concerning the zenith-sky simulations, the different models agree generally well, especially below 90° SZA. At higher SZA, larger discrepancies are obtained with relative differences ranging between 2% and 14% in some cases. In MAX geometry, good agreement is found between the models with the calculated NO₂ and HCHO SCDs differing by no more than 5% in the elevation and solar zenith angle (SZA) ranges investigated (5°–20° and 35°–85°, respectively). The impacts of aerosol scattering, ground albedo, and relative azimuth on MAX simulations have also been tested. Significant discrepancies appear for the aerosol effect, suggesting differences between models in the treatment of aerosol scattering. A bet-

ter agreement is found in case of the ground albedo and relative azimuth effects. The complete set of initialization data and results have been made publicly available through the QUILT project web site (<http://nadir.nilu.no/quilt/>), enabling the testing of other RT codes designed for the calculation of SCDs/AMFs.

1 Introduction

Since the middle of the 1970s, stratospheric ozone and several trace gases directly or indirectly involved in the ozone depletion like NO₂, BrO, and OClO have been monitored from the ground using the Differential Optical Absorption Spectroscopy (DOAS)-technique (Platt, 1994). A significant part of this monitoring effort has been carried out through the framework of the Network for the Detection of Stratospheric Change (NDSC). The NDSC consists of about 75 globally distributed stations combining various observation techniques. The network operation started in January 1991 and has been providing a consistent, standardised set of long-term measurements of stratospheric and, more recently, tropospheric trace gases, particles, and physical parameters for detecting atmospheric change, validating space-borne sensors, and testing and improving multidimensional models of both the stratosphere and troposphere (further information at <http://www.ndsc.ncep.noaa.gov/>). Concerning the scattered sunlight DOAS instruments, they operated until recently

Correspondence to: F. Hendrick
(franch@oma.be)

almost only in zenith-sky geometry, thus probing mainly the altitude region corresponding to the stratosphere, especially at large solar zenith angles (SZAs). Over the last decade, new instruments pointing not only at zenith but also towards the horizon (off-axis geometry) have been developed (e.g., Heckel et al., 2005; Hönninger et al., 2004; Wagner et al., 2004; Wittrock et al., 2004). Pointing at an elevation angle close to the horizon provides enhanced sensitivity to the troposphere compared to zenith-sky observations. The Multi-AXis (MAX-) DOAS technique combines different elevation angles. Owing to the variation of the light paths in the troposphere with the elevation angle, the different viewing directions have maximum sensitivity at different altitudes, thus providing some information on the vertical distribution of the absorber.

An important step in the interpretation of DOAS observations is the conversion of the slant column densities (SCDs) – which are the direct product of the DOAS analysis – into vertical column densities (VCDs) using calculated air mass factors (AMFs). The AMF represents the ratio of the effective optical path through the atmosphere to the vertical optical path and is given by the ratio SCD/VCD (Noxon et al., 1979; Solomon et al., 1987). In practice, AMFs are calculated using a radiative transfer (RT) model. In case of short lived species such as BrO, OCIO, and NO₂, the calculation of SCDs and therefore AMFs is complicated by the variation of the concentration of these species along a given light path due to the fast diurnal variation of these radicals coupled to the local SZA variation along the light path (Fish et al., 1995). This so-called photochemical enhancement effect is taken into account by initializing RT models with a table containing the concentrations of the absorber for different altitudes and SZAs. This table is then interpolated to determine the trace gas concentrations at the altitudes and local SZAs of the different scatter points considered along a given sun ray path. Such a concentration table is usually generated by running a stacked box photochemical model initialized with the output of a 3-D chemical transport model (CTM) corresponding to the day and location of interest. SCDs calculated by coupling a 3-D CTM to a photochemical box-/RT model interface can also be directly compared to observed SCDs. For example, Sinnhuber et al. (2002) compared ground-based zenith-sky UV-visible observations of BrO obtained at 11 sites with simulations from the 3-D CTM SLIMCAT (Chipperfield, 1999). The RT model used was based on the single scattering ray tracing scheme of Solomon et al. (1987). Recently, several groups have initiated AMF calculations in order to interpret MAX-DOAS measurements. Hönninger et al. (2004) have studied the behaviour of AMFs as a function of the solar zenith, elevation, and relative azimuth angles, ground albedo, and aerosol loading for several idealized trace gas profiles. For this purpose, they have used the RT model TRACY based on a Monte Carlo approach (von Friedeburg, 2003). This model has been also used by Wagner et al. (2004) to perform RT modelling for MAX-DOAS O₄

observations at different aerosol conditions. Sensitivity tests on O₄ AMFs were carried out by Wittrock et al. (2004) with SCIATRAN, a RT code based on a combined differential-integral approach involving the Picard iterative approximation (CDIPI) (Rozanov et al., 2000, 2001, 2005) and, as a first application, NO₂ profile information were derived from MAX-DOAS observations. It should be noted that an accurate RT model as forward model is essential in the retrieval of tropospheric trace gas profiles using MAX-DOAS measurements (e.g., Bruns et al., 2004). In Heckel et al. (2005), the SCIATRAN model also generated appropriate AMFs for the conversion of MAX-DOAS measurements of HCHO into VCDs. These examples show that RT modelling plays a central role in the interpretation of ground-based DOAS observations and that different RT computation schemes are available for this purpose.

The QUILT (Quantification and Interpretation of Long-Term UV-Vis Observations of the Stratosphere) project is an EU funded project based on the exploitation of the NDSC and aimed at quantifying ozone loss and investigating its relation to active halogen and nitrogen species using the existing ground-based, satellite and balloon borne UV-visible data as well as 3-D atmospheric modelling tools. One of the tasks of this project has been to test the consistency between the different RT models existing within the consortium and used to interpret the ground-based and satellite DOAS data. This objective has been achieved through several SCD simulations comparison tests performed using identical settings for all the models. Both ground-based zenith-sky (trace gases: BrO, NO₂, and OCIO) and MAX geometries (trace gases: NO₂ and HCHO) have been considered for these tests, with photochemical enhancement being taken into account only in zenith-sky geometry.

Here we report on the results of this intercomparison exercise. It should be noted that our study does not address the issue of the absolute accuracy of the SCD calculations, the consistency between simulated and measured SCDs having already been tested in several papers (e.g., Sinnhuber et al., 2002; Tørnkvist et al., 2002). It can be considered to a certain extent as the continuation of Sarkissian et al. (1995) who calculated O₃ and NO₂ AMFs with different RT models in zenith-sky geometry but without taking into account the photochemical enhancement effect (use of a single profile for the initialization of the models). Our paper is divided into five parts. In Sect. 2, we describe the different RT models involved in the intercomparison exercise. The comparison tests in zenith-sky and MAX geometries are described in Sects. 3 and 4, respectively, and their corresponding results are discussed therein. Sects. 5 and 6 are dedicated to the impact of aerosols and ground albedo on MAX simulations, respectively.

Table 1. Short description of the RT models involved in the intercomparison exercise. Note that both IASB and NILU models are based on the UVspec/DISORT package. However, they are not strictly identical since they have been adapted separately by each group in order to allow SCD/AMF calculations taking into account photochemical enhancement.

Group	Model main features	Scattering mode(s)	Reference(s)
UBRE	SCIATRAN model: –Combining Differential-Integral approach using the Picard-Iterative approximation (CDIPI) –Treatment of MS in a full spherical geometry including refraction –Chemistry included (2-D array of profile variation with SZA) –Treatments for aerosol and cloud scattering, and ground albedo –Possibility to include Raman scattering (but not used in the present study)	SS+MS	Rozanov et al. (2000, 2001, and 2005); Wittrock et al. (2004)
UHEI	TRACY model: –Backward Monte Carlo approach –Treatment of MS in a full spherical geometry including refraction –Chemistry included (2-D array of profile variation with SZA) –Treatments for aerosol and cloud scattering, and ground albedo –Possibility to include Raman scattering (but not used in the present study)	SS+MS (only MS in this study)	von Friedeburg (2003); Hönninger et al. (2004)
NILU and IASB	UVspec/DISORT package: –Discrete ordinate method –Chemistry included (2-D array of profile variation with SZA) –Treatment of MS and refraction in a pseudo-spherical geometry (direct beam only) –Treatments for aerosol and cloud scattering, and ground albedo	SS+MS	Mayer and Kylling (2005)
ISAC-CNR	AMEFCO model: –Single scattering model in a 2-D atmosphere (profile variation with SZA) –Treatment in full spherical geometry including refraction and aerosol scattering	SS	Petricoli et al. (2002a, b)
NIWA	–Single scattering model in a 2-D atmosphere (profile variation with SZA) –Treatment in full spherical geometry including refraction and aerosol scattering	SS	Schofield (2003); Schofield et al. (2004)

2 Description of the RT models

The groups contributing RT calculations to the intercomparison exercise were the remote sensing groups at the Universities of Bremen (UBRE) and Heidelberg (UHEI), the Norwegian Institute for Air Research (NILU), the Institute of Atmospheric Science and Climate (ISAC-CNR), the National Institute of Water and Atmospheric Research (NIWA), and the Institut d'Aéronomie Spatiale de Belgique (IASB). A summary of the characteristics of the models used by these groups is given in Table 1. From now on, each model will be referred to by the acronym of its corresponding group (in brackets here above). All models include the possibility of taking into account photochemical enhancement. The solution approaches to the RT equation (RTE) used in the different RT codes are as follows:

- The Combined Differential-Integral (CDI) approach (UBRE model): is based on the solution of the integral

RT equation using the characteristics method (Currant and Hilbert, 1962). The source function is integrated along the line of sight intersecting a spherical atmosphere. The single scattering part of the source function is calculated truly spherical and the multiple scattering part is initialized by the output of the pseudo-spherical model (Rozanov et al., 2000 and 2001).

- The Discrete Ordinate method (NILU and IASB models): the azimuth dependence of the radiation field is expressed as a Fourier cosine series in azimuth. The solution of the Fourier components is obtained using a numerical quadrature scheme, allowing to replace the integrals by sums and thus reducing the RTE to the solution of a set of coupled linear first-order differential equations (Lenoble, 1985; Stamnes et al., 1988; Spurr, 2001).
- The backward Monte Carlo method (UHEI model): a photon emerges from a detector in an arbitrary line of

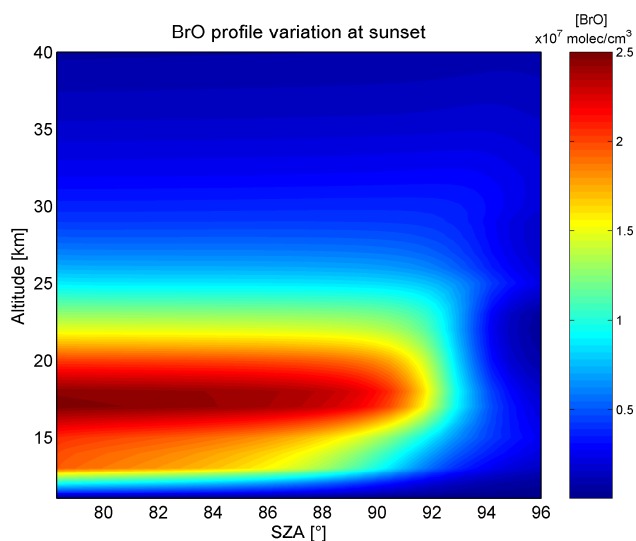


Fig. 1. Contour plot of the BrO profiles table used to initialize the models in the comparison test in zenith-sky geometry. The variation of the BrO profiles as a function of the SZA has been calculated for Harestua (60° N, Norway) at sunset under chlorine activated conditions.

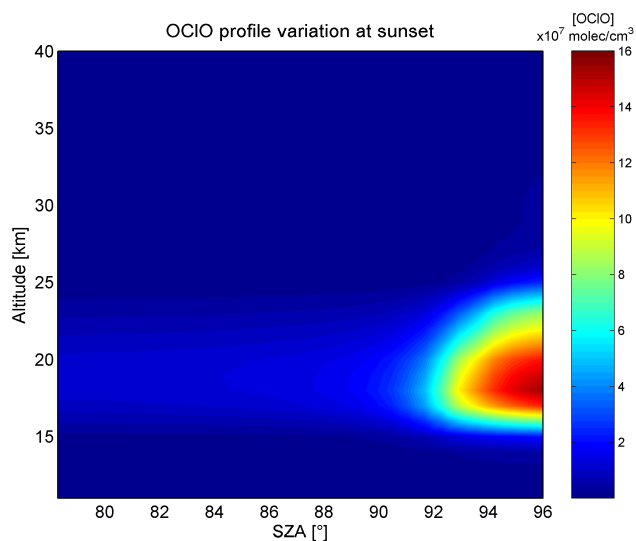


Fig. 2. Contour plot of the OCIO profiles table used to initialize the models in the comparison test in zenith-sky geometry. The variation of the OCIO profiles as a function of the SZA has been calculated for Harestua (60° N, Norway) at sunset under chlorine activated conditions.

sight direction and is followed in the backward direction along the path towards the sun. The various events which may happen to the photon at various altitudes in the atmosphere are defined by suitable probability distributions. Random numbers decide on the occurrence of events. At the location of the last scattering event prior to leaving the atmosphere, the impinging radiance

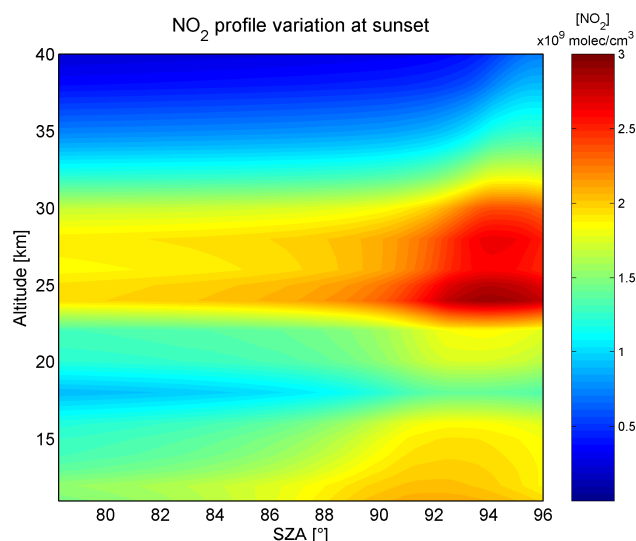


Fig. 3. Contour plot of the NO₂ profiles table used to initialize the models in the comparison test in zenith-sky geometry. The variation of the NO₂ profiles as a function of the SZA has been calculated for Harestua (60° N, Norway) at sunset in summer.

is calculated and weighted with the value of the scattering phase function and with the attenuation of the complete path. A large number of such random photon paths will reproduce the light contributing to the simulated measurement (von Friedeburg, 2003; Lenoble, 1985).

- Single scattering ray tracing method (ISAC-CNR and NIWA models): in zenith-sky geometry, it consists of computing the attenuation from the sun through discrete spherical atmospheric shells to “points” where the light beams are scattered into the detector (Solomon et al., 1987).

3 Zenith-sky simulations of BrO, NO₂, and OCIO SCDs including photochemical enhancement

3.1 Comparison test description

In this test, BrO, OCIO, and NO₂ SCDs have been calculated in zenith-sky geometry in single scattering (SS) and, when possible, in multiple scattering (MS) modes, taking into account photochemical enhancement effect. The settings imposed for all models are summarized in Table 2. Contour plots of the diurnal variation tables (concentration of BrO, OCIO, and NO₂ as a function of altitude and SZA) are shown in Figs. 1, 2, and 3, respectively. They are the output of the stacked box photochemical model PSCBOX (Errera and Fonteyn, 2001; Hendrick et al., 2000 and 2004) initialized with the 3-D-CTM SLIMCAT chemical and meteorological fields. Two scenarios have been considered: Harestua (60° N, Norway) at sunset in summer for NO₂ SCD

Table 2. Model settings for the comparison test in zenith-sky geometry. All the initialization data are available on the QUILT web site (<http://nadir.nilu.no/quilt/>).

Altitude grid	0–120 km/1 km thick
Wavelength	352 nm (BrO) 368 nm (OCIO) 422 nm (NO ₂)
Diurnal variation table (see Figs. 1, 2, and 3) p, T profiles	From PSCBOX model From SLIMCAT 3-D-CTM; interpolation using AFGL 1976 outside the SLIMCAT altitude range
O ₃ profile	From PSCBOX model; interpolation using AFGL 1976 outside the SLIMCAT altitude range
NO ₂ profile (for BrO and OCIO SCD calculations)	From PSCBOX model; interpolation using AFGL 1976 outside the SLIMCAT altitude range
Mie scattering	Not included
Refraction	Not included
Cross sections sets	BrO: Wahner et al. (1988) OCIO: Wahner et al. (1987) NO ₂ : Burrows et al. (1998) O ₃ : Burrows et al. (1999)
Ground albedo	0.20
Scattering mode	SS+if possible MS

calculations and Harestua at sunset under chlorine activated conditions for BrO and OCIO. All calculations included absorption by O₃ and, in case of BrO and OCIO, also absorption by NO₂.

3.2 Results

The results of the zenith-sky simulations of BrO, NO₂, and OCIO SCDs are presented in Fig. 4. We first concentrate on the general behaviour of the simulated SCDs. Figure 4 shows that the impact of MS is more important for BrO than for NO₂, and for OCIO, it is mostly significant at large SZA (>92°). The different behaviours of BrO and NO₂ regarding MS effects can be mainly attributed to the different wavelengths used for both calculations (352 nm for BrO and 422 nm for NO₂). In case of OCIO, the large impact of MS at SZAs larger than ~92° is related to the photochemistry of this species combined with geometrical considerations. Figure 2 shows that OCIO is situated in the ~17–22 km altitude range and only appears at SZAs > 92°. At these SZAs, the absorption due to OCIO along a given line of sight occurs where the local SZA is largest, i.e. near the vertical above the observing point. Thus, a significant part of the OCIO layer is likely to be in the Earth's shadow region where multiply scattered light has a stronger relative impact. This explains why the OCIO SCDs are so sensitive to MS in these conditions. The differences between the photochemical behaviours of BrO, NO₂, and OCIO are also manifest from

Fig. 4. BrO SCDs show a sharp decrease above ~92° SZA (see Fig. 1), consistent with the rapid conversion of BrO into its night-time reservoirs (mostly BrCl in the present case) in the absence of sunlight. In contrast, the concentrations of OCIO and NO₂ increase with SZA (see Figs. 2 and 3, respectively), which explains the persistence of relatively large SCD values at corresponding SZAs, especially in MS mode. However, OCIO and NO₂ SCDs also decrease at very high SZAs. This decrease happens when the mean scattering altitude moves above the trace gas layer. The SZA where the maximum SCD is reached is thus determined by a combination of photochemistry and altitude range of the trace gas layer.

Concerning the comparison of simulated SCDs, the relative differences between the results of the different models and those of IASB arbitrarily taken as reference, appear in the lower plots of Fig. 4 and a summary of the maximum differences found is presented in Table 3. In SS mode, good agreement is obtained below 90° SZA between the NIWA, IASB, NILU, and UBRE models: for the three species, the relative difference between the NIWA, NILU, and UBRE models and the IASB one (reference model) is smaller than 1%. However, the SCDs simulated by the ISAC-CNR model are systematically larger and the relative differences rise up to 4% for BrO, 5% for NO₂ and 7.5% for OCIO. Above 90° SZA, the agreement between the NIWA, IASB, UBRE, and NILU models is still very good with relative differences smaller than 1.8% for BrO, 1.3% for NO₂,

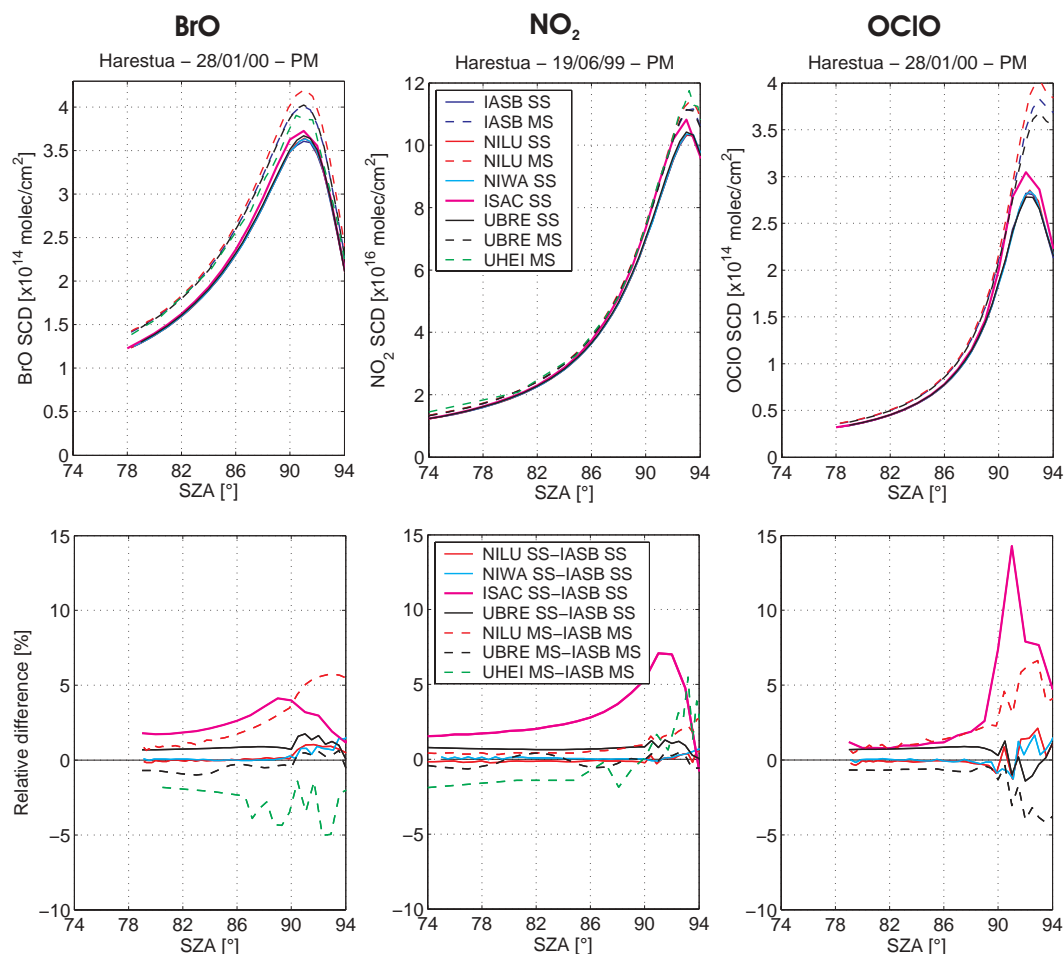


Fig. 4. Sunset BrO, NO₂, and OCIO SCDs calculated in the comparison test in zenith-sky geometry. The upper plots correspond to the SCDs and the lower plots to the relative differences between the results from the different models and those from the IASB model arbitrarily chosen as reference. Solid and dashed lines correspond to calculations in SS and MS modes, respectively. Note that the UHEI OCIO data are missing (see Sect. 3.2) and in the upper plots, the blue, red, and cyan solid lines corresponding to, respectively, the IASB, NILU, and NIWA SCD calculations in SS mode are almost superimposed.

Table 3. Maximum relative differences obtained between the different RT models and the IASB one – arbitrarily taken as reference – for the comparison test in zenith-sky geometry. Note that the SS and MS models have been compared to the IASB model in SS and MS modes, respectively.

	BrO [%]	NO ₂ [%]	OCIO [%]
NILU SS	+1.0	+0.5	+2.1
ISAC SS	+4.1	+7.1	+14.3
NIWA SS	+1.5	+0.7	+1.6
UBRE SS	+1.8	+1.3	−1.4
NILU MS	+5.8	+2.7	+6.6
UHEI MS	−5.0	+5.5	–
UBRE MS	−1.0	−0.6	−4.2

and 2.1% for OCIO. A maximum spread between models of about 2% is a better agreement than obtained by Sarkissian et al. (1995) without taking into account photochemical enhancement (from Sarkissian et al. (1995), the maximum spread values rise up to 13% for O₃ and 8% for NO₂ at 94° SZA). Concerning the ISAC-CNR simulations above 90° SZA, the discrepancies with the IASB model are larger than for the NIWA and NILU models: the relative differences are smaller than 4% for BrO and rise up to 7.1% for NO₂, and 14.3% for OCIO. Although these maximum relative differences are consistent with those of Sarkissian et al. (1995), they suggest that the ISAC-CNR model differs from the other models in the way the optical thickness of each atmospheric shell is calculated. Sarkissian et al. (1995) investigated the influence of the different methods used to interpolate the concentration and to calculate the geometrical path in individual shells. They found that the impact of these parameters

increases with increasing SZA and can reach 4% above 90° SZA. Since photochemical enhancement is included in the present test, we cannot neglect the impact of differences in interpolating the tables of photochemical species concentrations. This effect is consistent with the increase in the relative differences between the models with increasing SZA since the step between the SZA values corresponding to the concentration tables is increasing at large SZAs, due to the fact that the stacked box photochemical model PSCBOX provides output with a constant time step. Concerning the calculations in MS mode, the agreement below 90° SZA between the NILU, IASB, UBRE, and UHEI models is good since the relative differences with the IASB model results are smaller than 4.4%. Above 90° SZA, slightly larger discrepancies are generally found, as in SS mode, and the maximum relative differences with the IASB model results rise up to 6.6% for the NILU model (obtained for OCIO SCD calculations), 5.5% for the UHEI model (obtained for NO₂ SCD calculations), and 4.2% for the UBRE model (obtained for OCIO SCD calculations). It should be noted that UHEI OCIO data are absent from the comparison. This is caused by the fact that too many photons (around 10⁵) would have been required to calculate each SCD with sufficient accuracy and precision. In contrast to the NO₂ or BrO profile, stratospheric OCIO is usually confined to a layer of only a few kilometres thickness, and the concentration gradient is very high at its lower and upper ends (see Fig. 2). The Monte Carlo nature of the UHEI model causes statistical fluctuations (from photon path to photon path) of the altitude of the first scattering event the photon encounters after atmosphere entry. If this event occurs above the OCIO layer, then the path through this layer is short. If the event occurs within the OCIO layer, the light path through this layer is long. If the event occurs below the OCIO layer, then the path through the layer has also been long, though shorter than in the second case. Accordingly, small variations in the altitude of the first scattering event, arising from statistical fluctuations, lead to large variations in path length and hence to large fluctuations in the simulated SCD. This noise can only be reduced with a very large number of modelled photons, which causes the UHEI model to be inefficient for this specific kind of scenario. With the expected increase in computational power, this disadvantage is likely to become less significant in the near future.

4 Multi-axis simulations of NO₂ and HCHO SCDs

4.1 Comparison test description

In contrast to the zenith-sky simulations, photochemical enhancement has not been taken into account in the MAX simulations. The reason is that this effect becomes significant only during twilight, i.e. above 85° SZA, and we have limited our comparison to the 38°–85° SZA range because the sen-

sitivity of the MAX-DOAS observations to the troposphere is largest during daytime, i.e. at small SZA. The NO₂ and HCHO profiles used for the initialization of the models are shown in Fig. 5. All calculations included absorption by O₃ and in case of HCHO, also absorption by NO₂. SCD simulations have been performed for 5°, 10°, and 20° elevation above the horizon. For each elevation angle, four values of the azimuth angle of line of sight (AzLOS) have been considered: 30°, 60°, 90°, and 120°. The AzLOS is the relative azimuth angle between the pointing direction of the instrument and the sun azimuth. The other settings are shown in Table 4. Concerning the HCHO SCD calculations, the layer thickness in the altitude range where the concentration of this species changes rapidly with altitude (0–3 km) has been fixed to 0.2 km instead of the 1 km thickness used in case of NO₂, reducing interpolation effects. Only models enabling calculations in MS mode have been involved in this test since MS is the only acceptable scattering mode in MAX geometry (Wittrock et al., 2004). These models are: IASB, NILU, UBRE and UHEI.

4.2 Results

Figure 6 shows the results of the NO₂ and HCHO SCD simulations for 5°, 10°, and 20° elevation and 90° AzLOS. A summary of the maximum differences between the different models and the IASB one (again taken arbitrarily as reference model) is also presented in Table 5. The agreement between IASB, NILU, UBRE and UHEI is good: when comparing the results for both species over the whole SZA range and for all the elevation angles, the relative differences between the NILU, UBRE, and UHEI models and the IASB one are smaller than 5.1%. Concerning the UBRE model, it underestimates the IASB model results by at most 4.5% for NO₂ and 5.1% for HCHO. Furthermore, the relative differences are also almost constant over the whole SZA range. This is in contrast to the relative differences between the UHEI and IASB models which show a SZA dependence, especially at low elevation angles: e.g., for NO₂ at 5° elevation, the UHEI model results overestimate the IASB ones by 3% at 40° SZA and underestimate them by 3.6% at 85° SZA. However, with maximum relative differences of 3.8% for NO₂ and 4.5% for HCHO (see Table 5), the agreement between both models is good. As expected since they are both based on the UVspec/DISORT package, the NILU and the IASB models agree very well: for both NO₂ and HCHO, the relative difference between the results of both models is smaller than 1.3% over the entire SZA range and for all elevation angles.

The impact of the relative azimuth has been tested by calculating NO₂ and HCHO SCDs for different AzLOS values (30°, 60°, 90°, and 120°). The AzLOS effect on NO₂ SCDs is illustrated in Fig. 7 where the relative differences between the NO₂ SCDs at 30°, 60°, and 120° AzLOS and the SCD at 90° AzLOS (reference) are plotted as a function of SZA

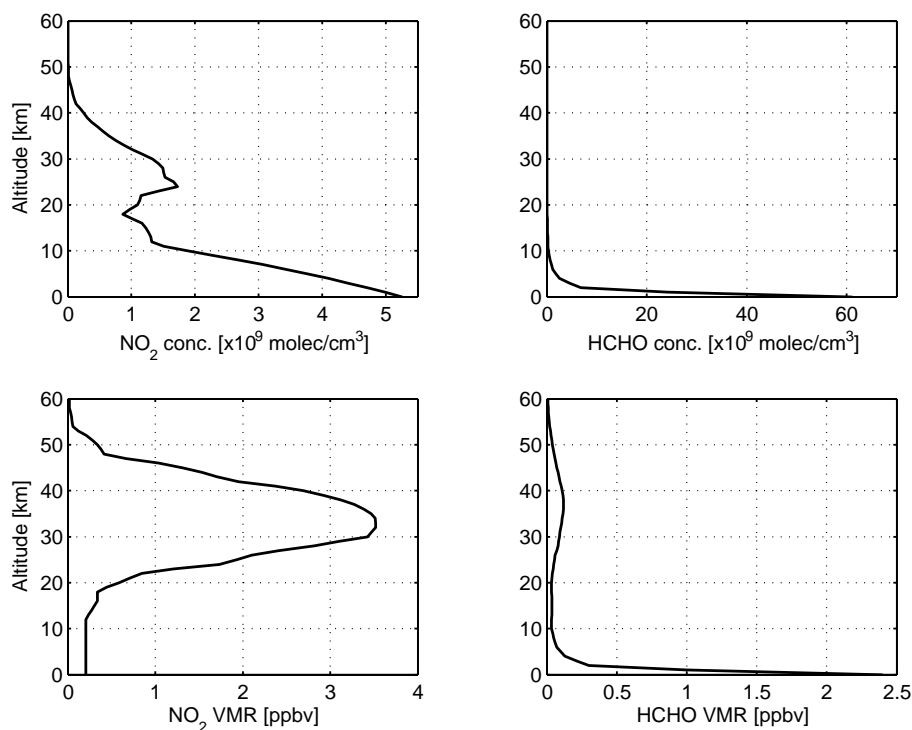


Fig. 5. NO₂ (left) and HCHO (right) profiles in concentration (upper plots) and VMR (lower plots) used to initialize the RT models in the comparison tests in MAX geometry.

Table 4. Model settings for the comparison test in MAX geometry. It should be noted that the same settings are used for the tests on aerosols effect (except Mie scattering is then included; see Sect. 5) and ground albedo effect (with the ground albedo value then fixed to 0 and 0.9 instead of 0.2; see Sect. 6). All the initialization data are available on the QUILT web site (<http://nadir.nilu.no/quilt/>).

Altitude grid	NO ₂ : 0–120 km/1 km thick HCHO: 0–120 km/0.2 km thick between 0 and 3 km and 1 km thick above 3 km
Wavelength	356 nm (HCHO) 422 nm (NO ₂)
p, T profiles	From SLIMCAT 3-D-CTM; interpolation using AFGL 1976 outside the SLIMCAT altitude range
O ₃ profile	From PSCBOX model; interpolation using AFGL 1976 outside the SLIMCAT altitude range
NO ₂ profile (for HCHO SCD calculations)	From PSCBOX model; interpolation using AFGL 1976 outside the SLIMCAT altitude range
HCHO and NO ₂ profiles (see Fig. 5)	HCHO: Barbe et al. (1979); Ehhalt and Tönnißen (1979) NO ₂ : from PSCBOX model
Mie scattering	Not included
Refraction	Not included
Cross sections sets	HCHO: Cantrell et al. (1990) NO ₂ : Burrows et al. (1998) O ₃ : Burrows et al. (1999)
Ground albedo	0.20
Elevation angle	5°, 10°, and 20°
Azimuth angle of line of sight	30°, 60°, 90°, and 120°
Scattering mode	MS

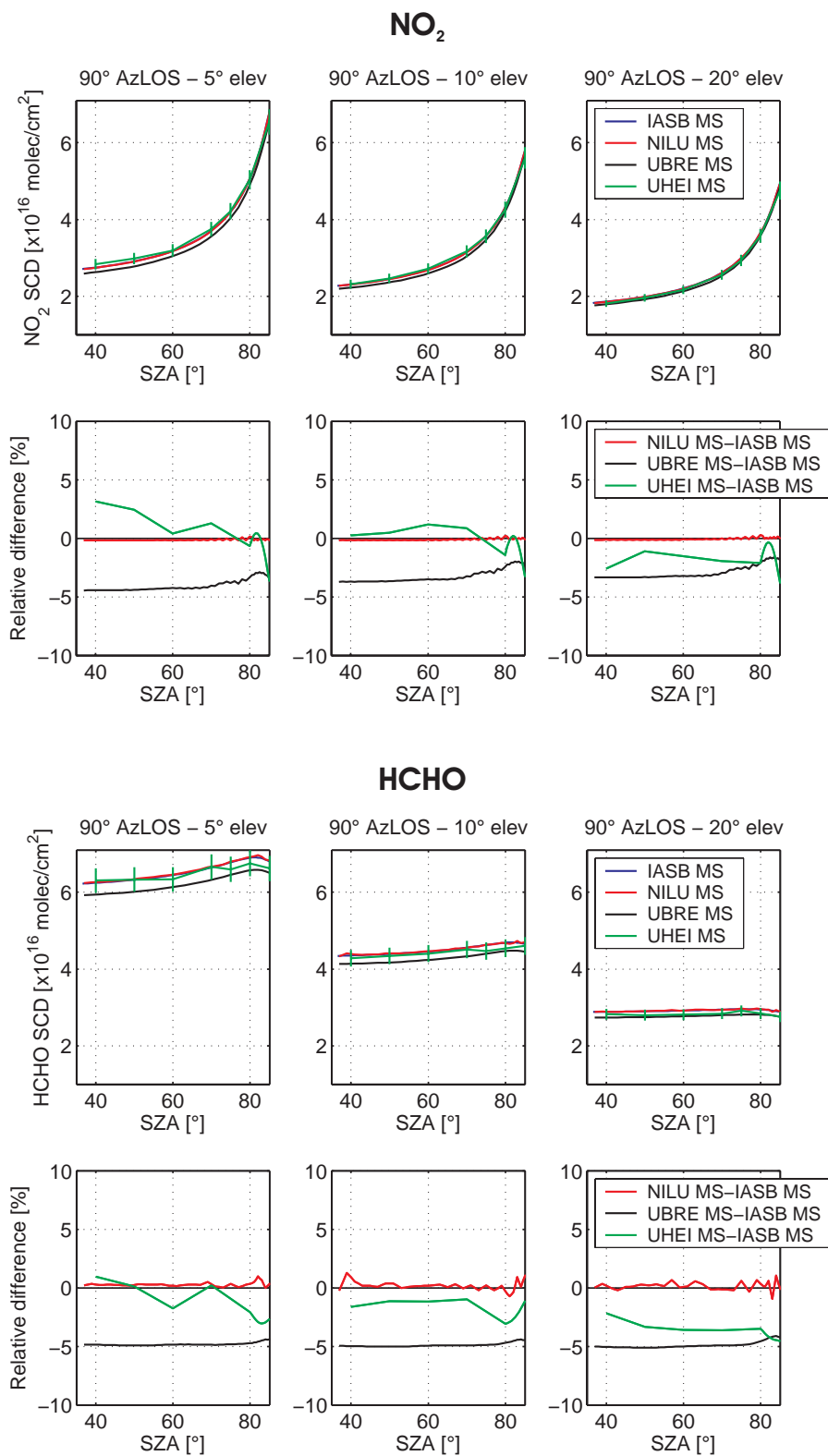
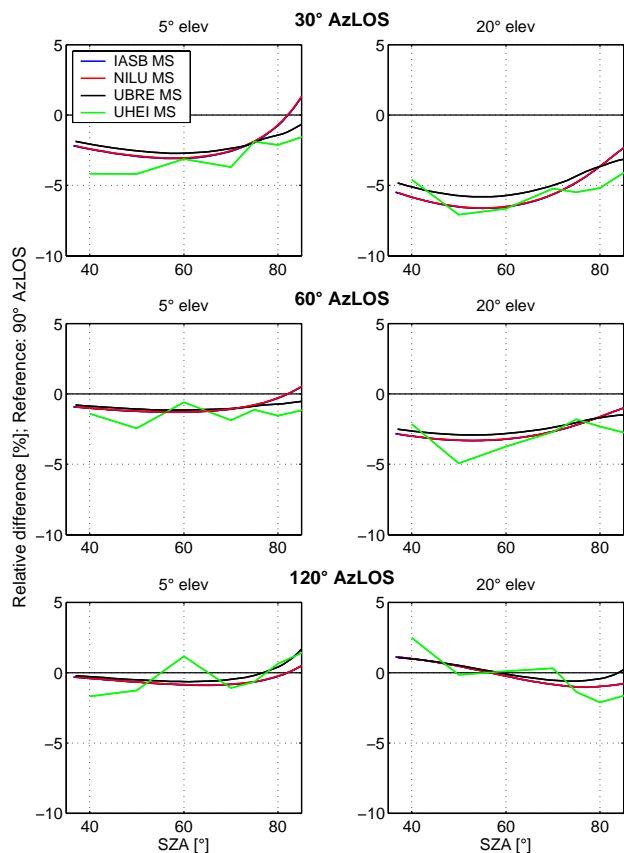


Fig. 6. NO₂ and HCHO SCDs calculated in MS mode in the comparison test in MAX geometry. For each species, the upper plots correspond to the SCDs and the lower plots to the relative differences between the different models and the IASB one arbitrarily chosen as reference. Results for 90° AzLOS and for 5°, 10°, and 20° elevation are plotted here.

Table 5. Maximum relative differences obtained between the different RT models and the IASB one – arbitrarily taken as reference – for the comparison test in MAX geometry.

		5° elevation [%]	10° elevation [%]	20° elevation [%]
NILU MS	NO ₂	−0.2	+0.2	+0.3
	HCHO	+1.0	+1.3	+1.1
UHEI MS	NO ₂	−3.6	−3.2	−3.8
	HCHO	−3.0	−3.0	−4.5
UBRE MS	NO ₂	−4.5	−3.7	−3.3
	HCHO	−5.0	−5.0	−5.1

**Fig. 7.** Impact of the relative azimuth on the NO₂ SCDs calculated in MAX geometry. The relative differences between the NO₂ SCDs calculated at 30° (upper plots), 60° (middle plots), and 120° (lower plots) AzLOS and those calculated at 90° AzLOS (reference case) are plotted here. Left and right plots correspond to results for 5° and 20° elevation, respectively. Note that the IASB blue lines are superimposed to the NILU red lines.

for 5° and 20° elevation. The largest AzLOS impact on NO₂ SCDs (7%) occurs at 50° SZA for 30° AzLOS and 20° elevation, i.e. at small AzLOS and high elevation angle. In case of HCHO (not shown here), the AzLOS effect is smaller by 1–2% compared to NO₂. It should be noted that a larger rel-

ative azimuth effect is expected in presence of aerosols, due to the strong preference of forward scattering by particles, whereas the Rayleigh phase function is symmetric in forward and backward directions. Concerning the consistency between the IASB, NILU, UBRE, and UHEI models with respect to the impact of the AzLOS, Fig. 7 shows that they agree reasonably well.

5 Impact of aerosol scattering on multi-axis simulations of NO₂ and HCHO SCDs

Aerosols have a strong impact on MAX-DOAS observations (Wagner et al., 2004; Wittrock et al., 2004; and Heckel et al., 2005). The most important effect of the aerosol extinction is a reduction of the visibility of the atmosphere and thus a limitation by scattering of the light path of the lowest viewing directions, reducing the difference in tropospheric absorption path between the viewing directions. It has been shown by Wagner et al. (2004) that the impact of aerosols on O₄ SCDs can provide a new method to derive information on atmospheric aerosols.

In the present study, MAX NO₂ and HCHO SCDs have been simulated with and without aerosol scattering in order to test the consistency between the different RT models regarding the impact of aerosols in this geometry. The aerosol settings are shown in Fig. 8 (profiles of the extinction and absorption coefficients) and Table 6 (asymmetry factor). They have been constructed from the aerosol model of Shettle (1989) included in the IASB and NILU RT models using a surface visibility of 100 km. The settings in the boundary layer and troposphere correspond to mixture of water soluble and dust-like aerosols representative of a rural environment (low aerosol content). In the stratosphere, sulphuric acid aerosol settings corresponding to summer background conditions have been used. The other initialization parameters are the same as described in Sect. 4.1, except that HCHO and NO₂ SCDs have been calculated only for 90° AzLOS.

Figure 9 shows MAX NO₂ and HCHO SCDs simulated with and without aerosol scattering. Qualitatively, the impact of aerosols is the same for all models: a decrease of NO₂ and HCHO SCDs occurs when aerosol scattering is included

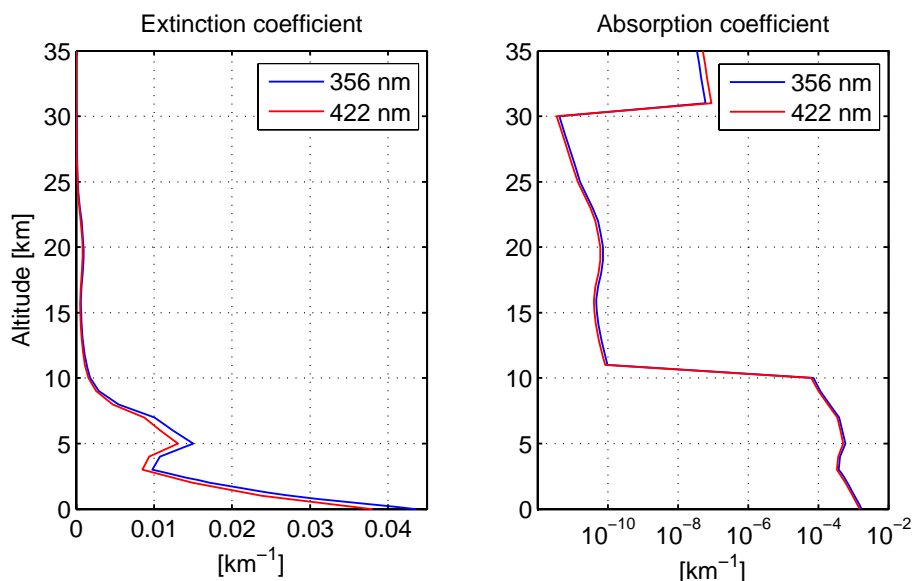


Fig. 8. Profiles of the aerosol extinction (left) and absorption (right) coefficients used for testing the impact of aerosols on MAX simulations of HCHO (356 nm) and NO₂ (422 nm) SCDs, respectively.

in the calculations. The presence of aerosols leads to a reduction of the direct light path, especially in the lowest layers, and therefore the absorption by NO₂ and HCHO is reduced (Wagner et al., 2004). The impact of aerosol scattering also decreases at higher elevation angles, due to the fact that, as the elevation angle increases, the mean scattering height increases and therefore the MAX SCD simulations become less sensitive to the lowest layers where the aerosol effect is largest.

When SCDs calculated with aerosols are compared, the different models agree reasonably well: they differ by 9% at most, which is of the same order of magnitude as the differences found for calculations without aerosols (5%, see Sect. 4.2). However, regarding the quantitative impact of the aerosol scattering, expressed in Fig. 9 by the relative differences between simulations with and without aerosol scattering, the models differ significantly. For example, in HCHO SCD simulations at 5° elevation, an aerosol impact of about 10% is found with the UHEI and UBRE models, which is twice as much as the impact obtained with the NILU and IASB models. In case of NO₂, such a difference is found between the UBRE and UHEI model results (see results for 5° elevation in Fig. 9). Figure 9 also shows that the impact of aerosol scattering is larger on NO₂ than on HCHO SCDs: the relative differences between calculations with and without aerosol scattering range for all models, elevation angles, and SZAs between −21% and +4% for NO₂ and between −13% and +1.5% for HCHO. These discrepancies obtained between the different models could not be resolved satisfactorily so far. It may be related to the different approximations used in the models for resolving the RT equation. For exam-

Table 6. Profiles of asymmetry factor used for testing the impact of aerosols on MAX simulations of HCHO (356 nm) and NO₂ (422 nm) SCDs.

	Asymmetry factor 356 nm	Asymmetry factor 422 nm
0–10 km	0.661	0.652
11–30 km	0.698	0.693
>30 km	0.701	0.698

ple, the UBRE and UHEI models are spherical whereas the NILU and IASB models use the pseudo-spherical approximation. A Fourier expansion is also applied in the NILU and IASB models, which could lead to a loss of angular information if too few Fourier terms are considered. In order to progress further in our understanding of the persistent discrepancies regarding the aerosol impact, a thorough examination of individual aerosol routines and additional comparison tests appear to be needed, which is beyond the scope of the present intercomparison exercise. This issue, and more generally the impact of aerosol scattering on MAX DOAS AMF simulations, is addressed more thoroughly as part of a new exercise, currently led by the University of Heidelberg in the framework of the European Network of Excellence on Atmospheric Composition ACCENT. More details on this new exercise as well as preliminary results can be found on the following web page: http://satellite.iup.uni-heidelberg.de/index.php/RTM_Workshop/149/0/.

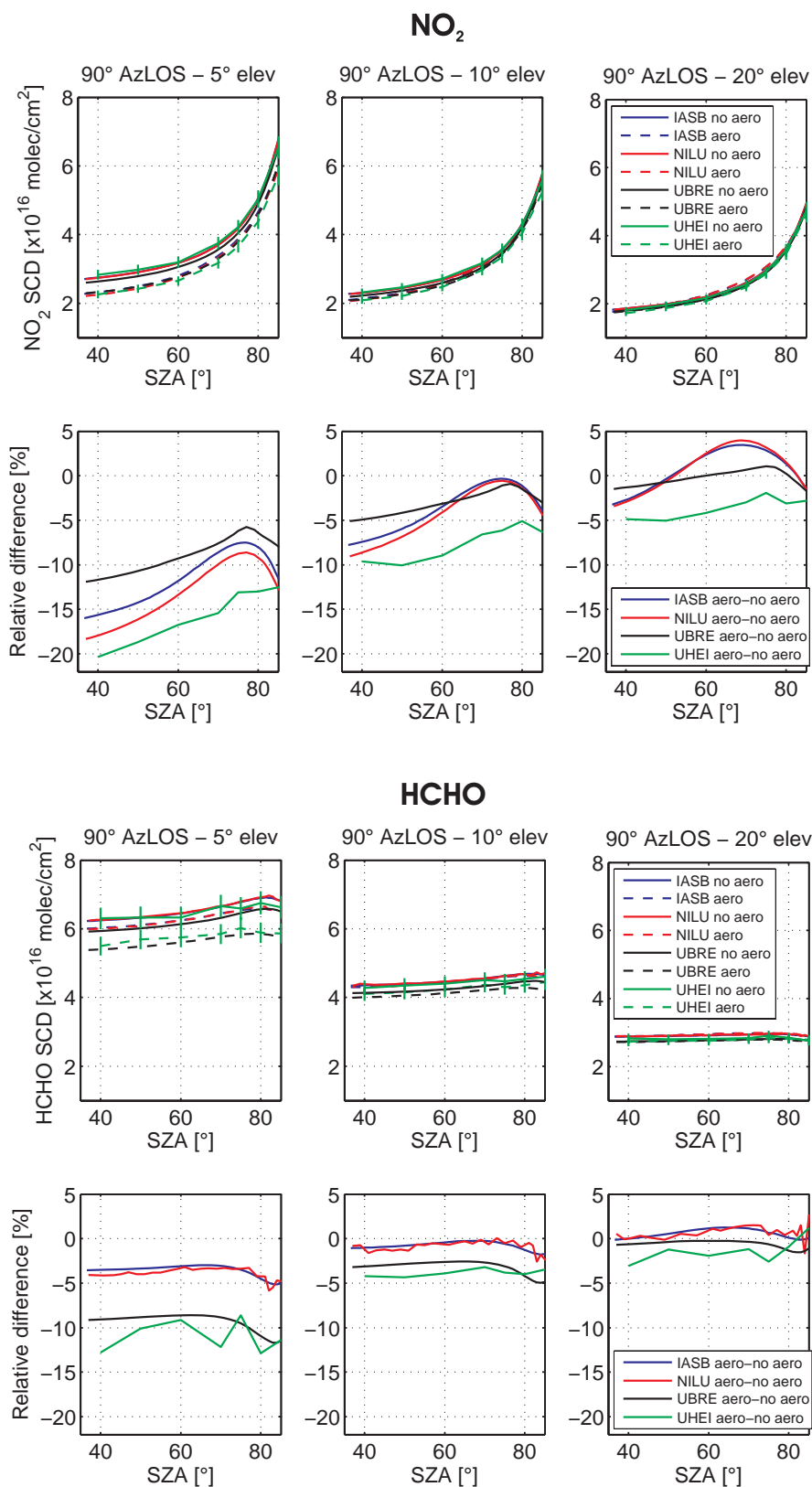


Fig. 9. Impact of aerosol scattering on simulated MAX NO₂ and HCHO SCDs. For each species, the upper plots correspond to the SCDs and the lower plots to the relative differences between SCDs calculated with and without aerosol scattering (reference: without aerosol scattering). Results for 90° AzLOS and for 5°, 10°, and 20° elevation are plotted here.

6 Impact of ground albedo on multi-axis simulations of NO₂ and HCHO SCDs

Ground albedo has a significant impact on the radiative transfer close to the ground (Hönninger et al., 2004; Wittrock et al., 2004). It is particularly important to properly estimate this parameter for observational sites displaying large albedo changes depending on the season or viewing direction. The main effect of an increase of the albedo is an increase of the number of scattering events in the layers close to the surface, resulting in longer absorption paths at these altitudes and therefore in higher absolute AMFs. However, the difference in AMF between off-axis and zenith-sky viewing directions is reduced, owing to the fact that the enhancement of the optical path with increasing albedo is largest for zenith-sky observations (Wittrock et al., 2004).

In order to test the consistency between the different RT models regarding the impact of the ground albedo in MAX geometry, NO₂ and HCHO SCDs have been simulated with ground albedo values fixed to 0 and 0.9. The other model settings are the same as those described in Sect. 4.1. As for the test on the impact of aerosol scattering, simulations have been performed only for 90° AzLOS.

Figure 10 illustrates the ground albedo effect on simulated MAX HCHO and NO₂ SCDs. The UBRE, NILU, and IASB models show excellent consistency with similar HCHO and NO₂ SCD increases being obtained with the three models. An increase in surface albedo value from 0.0 to 0.9 leads to an increase of the HCHO SCD of about 20% and 55% at 80° SZA for 5° and 20° elevation, respectively, whereas the NO₂ SCD increases by 5% and 12% under the same conditions. The fact that the HCHO SCDs are more sensitive to the ground albedo is expected since for the present simulations, HCHO, in contrast to NO₂, is mostly located in the lower part of the troposphere (between 0 and 5 km). In case of the UHEI model, the SCDs simulated for a surface albedo value of 0.0 agree reasonably well with the results from the other models. This agreement is similar to the one obtained for medium (0.2) surface albedo conditions (see Sect. 4). For very high surface albedo (0.9), the UHEI model gives generally larger SCD values, especially above 70° SZA. However, in case of HCHO SCDs, the differences between the UHEI model results and the analytical models results are similar to the differences found between the SCDs calculated by the three analytical models. Due to the larger SCD values obtained when surface albedo is fixed to 0.9, the UHEI model gives a significantly larger relative increase in SCDs compared to the other models: when the surface albedo increases from 0.0 to 0.9, the SCD increases at 80° SZA for 5° and 20° elevation reach 32% and 84% for HCHO, and 12% and 35% for NO₂. This behaviour could be related to the fact that the modelling of the absolute radiance still poses a challenge to backward Monte Carlo approaches, which is also under investigation by other groups. At high albedo, light reflected off the ground is unattenuated and increases the signal of ab-

sorbers near the ground, so the absolute radiance begins to play a significant role in the SCD calculations. The present intercomparison exercise was aimed at detecting those subtle effects, and the results will help to optimize the modelling. So will comparison with measurements, e.g., as performed in Weidner et al. (2005).

7 Conclusions

In the present intercomparison exercise, we have tested the consistency between six RT models used for interpreting ground-based zenith-sky and MAX-DOAS observations in the QUILT EU project. In the context of this project based on the exploitation of the NDSC, the comparison and optimization of these RT models is of central importance in order to provide accurate time-series of ground-based DOAS observations. This study represents a step forward with respect to previously published work in that it compares RT models in MAX geometry and takes into account photochemical enhancement effect for calculating SCDs of rapidly photolysing species in zenith-sky geometry.

Comparisons of NO₂ and HCHO SCDs in MAX geometry and multiple scattering mode without aerosol scattering show good agreement between all involved models: the calculated NO₂ and HCHO SCDs differ generally by no more than 5% in the SZA and elevation angle ranges investigated (35°–85° and 5°–20°, respectively). The impacts of the relative azimuth, aerosol scattering, and ground albedo on NO₂ and HCHO SCDs have been also quantitatively determined. The azimuth effect is found to be the largest at small AzLOS and high elevation angles. The maximum differences relative to 90° AzLOS in the 30°–120° AzLOS range and for 20° elevation rising up to 7% and 5% for NO₂ and HCHO SCDs, respectively. The models have also shown reasonably good consistency concerning this effect. This is in contrast to the aerosol scattering effect for which significant discrepancies still persist. Since all codes have been initialized identically, this result suggests that significant differences exist between the models regarding the treatment of aerosol scattering, may be related to the different approximations used for resolving the RT equation. This issue, and more generally the impact of aerosol scattering on the MAX DOAS AMF simulations, is addressed more thoroughly as part of a new intercomparison exercise, currently led by the University of Heidelberg in the framework of the European Network of Excellence ACCENT. More details on this new exercise as well as preliminary results can be found on the following web page: http://satellite.iup.uni-heidelberg.de/index.php/RTM_Workshop/149/0/. In the test on the impact of the ground albedo, very good agreement has been achieved between the IASB, NILU, and UBRE models whereas the albedo effect is significantly larger using the UHEI model, which is based on a Monte Carlo approach. It should be noted that the conclusions drawn here on the

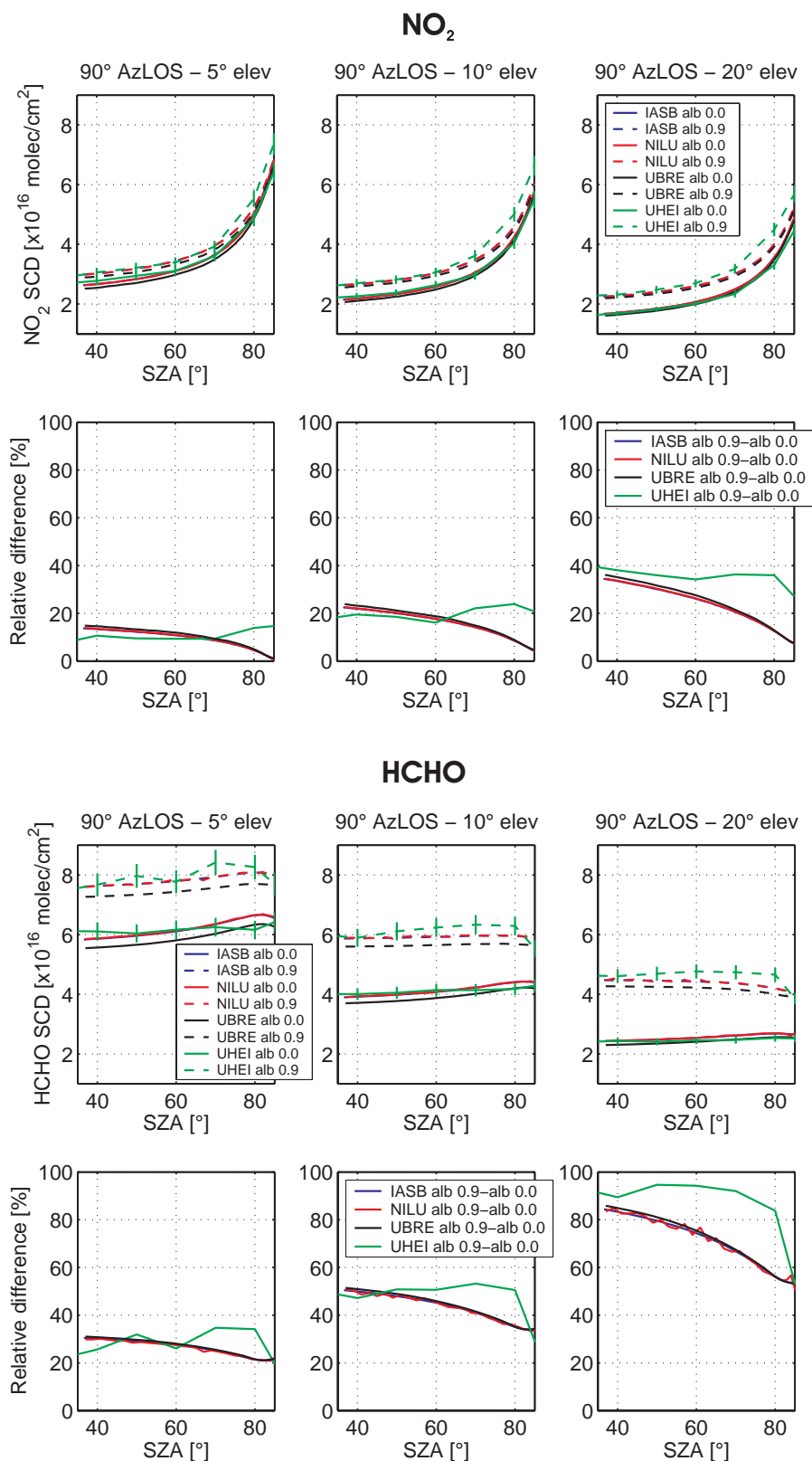


Fig. 10. Impact of the ground albedo on simulated MAX NO₂ and HCHO SCDs. For each species, the upper plots correspond to the SCDs and the lower plots to the relative differences between SCDs calculated with ground albedo values of 0.9 and 0.0 (reference: albedo=0.0). Results for 5°, 10°, and 20° elevation and 90° AzLOS are plotted here.

levels of agreement between models in the different comparison tests depend on the assumptions made for the vertical profiles. In case of NO₂ and HCHO, very different vertical profiles are indeed possible and could lead to different levels of agreement.

The comparisons of zenith-sky BrO, NO₂, and OCIO SCDs calculated in both single and multiple scattering modes show good overall agreement to a level that is consistent and in some cases better than in the Sarkissian et al. (1995) work. In single scattering mode, the relative difference between the models is smaller than 1% below 90° SZA, except for the ISAC-CNR model, for which relative differences rising up to 7.5% have been found in this SZA range. Above 90° SZA, the agreement between the IASB, NILU, UBRE, and NIWA models is still very good with a maximum spread of about 2%. Larger discrepancies have been obtained with the ISAC-CNR model, especially in the OCIO SCD calculations (relative difference with the IASB model up to 14%). These discrepancies could be partly due to differences in calculating the density in individual atmospheric shells. In multiple scattering mode, the differences between the NILU, UHEI, and UBRE models and the IASB one are smaller than 4.4% below 90° SZA for the three species. Above 90° SZA, slightly larger discrepancies have been obtained with a maximum relative difference with the IASB model of about 6.5%. As in MAX geometry, the assumptions made on the vertical profiles used for the zenith-sky simulations can have an impact on the agreement found between the models. This is particularly true for OCIO, for which a small change in the vertical profiles could change the behaviour of the different models.

The complete set of initialization data (profiles and cross sections sets) and results of this intercomparison exercise have been gathered in a “RT model validation package” enabling the testing of other RT codes aiming to the calculation of SCDs/AMFs. This validation package has been made publicly available through the QUILT project web site (<http://nadir.nilu.no/quilt/>).

Acknowledgements. This research was financially supported by the European Commission (contract QUILT, EVK2-2000-00545) and the Belgian Federal Science Policy Office (contracts ESAC II EV/35/3A and MO/35/006 & 012). M. P. Chipperfield (University of Leeds) is acknowledged for providing us with the SLIMCAT data. We would like also to thank the coordinators of the QUILT EC project, B. Arlander and G. O. Braathen (NILU).

Edited by: U. Pöschl

References

- Barbe, A., Marché, P., Secroun, C., and Jouve, P.: Measurements of tropospheric and stratospheric H₂CO by an infrared high resolution technique, *Geophys. Res. Lett.*, 6(6), 463–465, 1979.
- Bruns, M., Buehler, S. A., Burrows, J. P., Heue, K.-P., Platt, U., Pundt, I., Richter, A., Rozanov, A., Wagner, T., and Wang, P.: Retrieval of profile information from airborne multi-axis UV-visible skylight absorption measurements, *Appl. Opt.*, 43(22), 2004.
- Burrows, J. P., Dehn, A., Deters, B., Himmelmann, S., Richter, A., Voigt, S., and Orphal, J.: Atmospheric remote-sensing reference data from GOME: Part 1. Temperature dependent absorption cross sections of NO₂ in the 231–794 nm range, *J. Quant. Spectrosc. Radiat. Transfer*, 60, 1025–1031, 1998.
- Burrows, J. P., Richter, A., Dehn, A., Deters, B., Himmelmann, S., Voigt, S., and Orphal, J.: Atmospheric remote-sensing reference data from GOME: Part 2. Temperature dependent absorption cross sections of O₃ in the 231–794 nm range, *J. Quant. Spectrosc. Radiat. Transfer*, 61, 509–517, 1999.
- Cantrell, C. A., Davidson, J. A., McDaniel, A. H., Shetter, R. E., and Calvert, J. G.: Temperature-dependent formaldehyde cross sections in the near-ultraviolet region, *J. Phys. Chem.*, 94, 3902–3908, 1990.
- Chipperfield, M. P.: Multiannual simulations with a three-dimensional chemical transport model, *J. Geophys. Res.*, 104(D1), 1781–1805, 1999.
- Currant, R. and Hilbert, D.: *Methods of Mathematical Physics*, vol. 2, Interscience, New York, 1962.
- Errera, Q. and Fonteyn, D.: Four-dimensional variational chemical assimilation of CRISTA stratospheric measurements, *J. Geophys. Res.*, 106(D11), 12 253–12 265, 2001.
- Ehhalt, D. H. and Tönnißen, A.: Hydrogen and carbon compounds in the stratosphere, *Proceedings of the NATO Advanced Study Institute on Atmospheric Ozone: Its Variation and Human Influences*, edited by: Aikin, A. C., Report No. FAA-EE-80-20, U.S. Federal Aviation Administration, 1979.
- Fish, D. J., Jones, R. L., and Strong, E. K.: Midlatitude observations of the diurnal variation of stratospheric BrO, *J. Geophys. Res.*, 100(D9), 18 863–18 871, 1995.
- Hendrick, F., Mueller, R., Sinnhuber, B.-M., Bruns, M., Burrows, J. P., Chipperfield, M. P., Fonteyn, D., Richter, A., Van Roozendaal, M., and Wittrock, F.: Simulation of BrO Diurnal Variation and BrO Slant Columns: Intercomparison Exercise Between Three Model Packages, *Proceedings of the 5th European Workshop on Stratospheric Ozone*, Saint Jean de Luz, France, 27 Sept.–1 Oct. 1999, Air Pollution Research Report no. 73, European Commission – DG XII, Brussels, 2000.
- Hendrick, F., Barret, B., Van Roozendaal, M., Boesch, H., Butz, A., De Mazière, M., Goutail, F., Hermans, C., Lambert, J.-C., Pfeilsticker, K., and Pommereau, J.-P.: Retrieval of nitrogen dioxide stratospheric profiles from ground-based zenith-sky UV-visible observations: validation of the technique through correlative comparisons, *Atmos. Chem. Phys.*, 4, 2091–2106, 2004, **SRef-ID: 1680-7324/acp/2004-4-2091**.
- Heckel, A., Richter, A., Tarsu, T., Wittrock, F., Hak, C., Pundt, I., Junkermann, W., and Burrows, J. P.: MAX-DOAS measurements of formaldehyde in the Po-Valley, *Atmos. Chem. Phys.*, 5, 909–918, 2005, **SRef-ID: 1680-7324/acp/2005-5-909**.
- Hönninger, G., Friedeburg, C. V., and Platt, U.: Multi Axis Differential Optical Absorption Spectroscopy (MAX-DOAS), *Atmos. Chem. Phys.*, 4, 231–254, 2004, **SRef-ID: 1680-7324/acp/2004-4-231**.

- Lenoble, J.: Radiative Transfer in Scattering and Absorbing Atmospheres: Standard computational procedures, A. Deepak Publishing, Hampton, Virginia USA, 1985.
- Mayer, B. and Kylling, A.: Technical note: The libRadtran software package for radiative transfer calculations – description and examples of use, *Atmos. Chem. Phys.*, 5, 1855–1877, 2005, **SRef-ID: 1680-7324/acp/2005-5-1855**.
- Noxon, J. F., Whipple, E. C., and Hyde, R. S.: Stratospheric NO₂. 1. Observational method and behaviour at midlatitudes, *J. Geophys. Res.*, 84, 5047–5076, 1979.
- Petrìtoli, A., Ravegnani, F., Giovanelli, G., Bortoli, D., Bonafè, U., Kostadinov, I., and Oulanovsky, A.: Off-axis measurements of atmospheric trace gases by use of an airborne ultraviolet-visible spectrometer, *Appl. Opt.*, 41(27), 5593–5599, 2002a.
- Petrìtoli, A., Giovanelli, G., Kostadinov, I., Ravegnani, F., Bortoli, D., Bonasoni, P., Evangelisti, F., Bonafè, U., and Calzolari, F.: Tropospheric and stratospheric NO₂ amount deduced by slant column measurements at Mt. Cimone station, *Adv. Space Res.*, 29(11), 1691–1695, 2002b.
- Platt, U.: Differential optical absorption spectroscopy (DOAS), in: *Air Monitoring by Spectroscopic Techniques*, Chem. Anal. Ser., edited by: Sigrist, M. W., John Wiley, New York, 127, 27–84, 1994.
- Rozanov, A., Rozanov, V.-V., and Burrows, J.-P.: Combined differential-integral approach for the radiation field computation in a spherical shell atmosphere: Nonlimb geometry, *J. Geophys. Res.*, 105, D18, 22937, 2000.
- Rozanov, A., Rozanov, V.-V., and Burrows J.-P.: A numerical radiative transfer model for a spherical planetary atmosphere: combined differential-integral approach involving the Picard iterative approximation, *J. Quant. Spectrosc. Radiat. Transfer*, 69, 491, 2001.
- Rozanov, A., Rozanov, V., Buchwitz, M., Kokhanovsky, A., and Burrows, J. P.: SCIATRAN 2.0. A new radiative transfer model for geophysical applications in the 175–2400 nm spectral region, *Adv. Space Res.*, 36(5), 1015–1019, 2005.
- Sarkissian, A., Roscoe, H. K., Fish, D., Van Roozendael, M., Gil, M., Chen, H. B., Wang, P., Pommereau, J.-P., and Lenoble, J.: Ozone and NO₂ air-mass factors for zenith-sky spectrometers: Intercomparison of calculations with different radiative transfer models, *Geophys. Res. Lett.*, 22(9), 1113–1116, 1995.
- Schofield, R.: The vertical distribution of atmospheric BrO from ground-based measurements, PhD thesis, University of Auckland, Auckland, 2003.
- Schofield, R., Connor, B. J., Kreher, K., Johnston, P. V., and Rodgers, C. D.: The retrieval of profile and chemical information from ground-based UV-visible spectroscopic measurements, *J. Quant. Spectrosc. Radiat. Transfer*, 86, 115–131, 2004.
- Shettle, E. P.: Models of aerosols, clouds, and precipitation for atmospheric propagation studies, AGARD Conference Proceedings No. 454: Atmospheric propagation in the UV, visible, IR and mm-region and related system aspects, 1989.
- Sinnhuber, B.-M., Arlander, D. W., Bovensmann, H., Burrows, J. P., Chipperfield, M. P., Enell, C.-F., Frieß, U., Hendrick, F., Johnston, P. V., Jones, R. L., Kreher, K., Mohamed Tahrin, N., Müller, R., Pfeilsticker, K., Platt, U., Pommereau, J.-P., Pundt, I., Richter, A., South, A. M., Tørnkqvist, K.K., Van Roozendael, M., Wagner, T., and Wittrock, F.: Comparison of measurements and model calculations of stratospheric bromine monoxide, *J. Geophys. Res.*, 107(D19), 4398, doi:10.1029/2001JD000940, 2002.
- Solomon, S., Schmeltekopf, A. L., and Sanders, R. W.: On the Interpretation of Zenith sky Absorption Measurements, *J. Geophys. Res.*, 92(D7), 8311–8319, 1987.
- Spurr, R. J. D.: Linearized Radiative Transfer Theory: A general discrete ordinate approach to the calculation of radiances and analytic weighting functions, with application to atmospheric remote sensing, PhD thesis, Technische Universiteit Eindhoven, 2001.
- Stamnes, K., Tsay, S.-C., Wiscombe, W., and Jayaweera, K.: Numerically stable algorithm for discrete-ordinate-method radiative transfer in multiple scattering and emitting layered media, *Appl. Opt.*, 27, 2505–2509, 1988.
- Tørnkqvist, K. K., Arlander, D. W., and Sinnhuber, B.-M.: Ground-based UV measurements of BrO and OClO over Ny-Ålesund during Winter 1996 and 1997 and Andøya during Winter 1998/99, *J. Atmos. Chem.*, 43(2), 75–106, 2002.
- von Friedeburg, C.: Derivation of Trace Gas Information combining Differential Optical Absorption Spectroscopy with Radiative Transfer Modelling, PhD thesis, University of Heidelberg, 2003.
- Wagner, T., Dix, B., Friedburg, C. v., Frieß, U., Sanghavi, S., Sireich, R., and Platt, U.: MAX-DOAS O₄ measurements: A new technique to derive information on atmospheric aerosols-Principles and information content, *J. Geophys. Res.*, 109, D22205, doi:10.1029/2004JD004904, 2004.
- Wahner, A., Ravishankara, A. R., Sander, S. P., and Friedl, R.R.: Absorption cross-section of BrO between 312 and 385 nm at 298 and 223 K, *Chem. Phys. Lett.*, 152, 507–512, 1988.
- Wahner, A., Tyndall, G. Y., and Ravishankara, A. R.: Absorption cross-section for OClO as a function of temperature in the wavelength range from 240–490 nm, *J. Phys. Chem.*, 91, 2735–2738, 1987.
- Weidner, F., Bösch, H., Bovensmann, H., Burrows, J. P., Butz, A., Camy-Peyret, C., Dorf, M., Gerilowski, K., Gurlit, W., Platt, U., von Friedeburg, C., Wagner, T., and Pfeilsticker, K.: Balloon-borne Limb profiling of UV/vis skylight radiances, ozone and nitrogen dioxide: Technical set-up and validation of the method, *Atmos. Chem. Phys.*, 5, 1409–1422, 2005, **SRef-ID: 1680-7324/acp/2005-5-1409**.
- Wittrock, F., Oetjen, H., Richter, A., Fietkau, S., Medeke, T., Rozanov, A., and Burrows, J. P.: MAX-DOAS measurements of atmospheric trace gases in Ny-Ålesund – Radiative transfer studies and their application, *Atmos. Chem. Phys.*, 4, 955–966, 2004, **SRef-ID: 1680-7324/acp/2004-4-955**.